

Nonlinear, electrocatalytic swimming in the presence of salt

Benedikt Sabass¹ and Udo Seifert¹

II. Institut für Theoretische Physik, Universität Stuttgart, 70550 Stuttgart, Germany

A small, bimetallic particle in a hydrogen peroxide solution can propel itself by means of an electrocatalytic reaction. The swimming is driven by a flux of ions around the particle. We model this process for the presence of a monovalent salt, where reaction-driven proton currents induce salt ion currents. A theory for thin diffuse layers is employed, which yields nonlinear, coupled transport equations. The boundary conditions include a compact Stern layer of adsorbed ions. Electrochemical processes on the particle surface are modeled with a first order reaction of the Butler-Volmer type. The equations are solved numerically for the swimming speed. An analytical approximation is derived under the assumption that the decomposition of hydrogen peroxide occurs mainly without inducing an electric current. We find that the swimming speed increases linearly with hydrogen peroxide concentration for small concentrations. The influence of ion diffusion on the reaction rate can lead to a concave shape of the function of speed vs. hydrogen peroxide concentration. The compact layer of ions on the particle diminishes the reaction rate and consequently reduces the speed. Our results are consistent with published experimental data.

PACS numbers: 47.63.mf, 47.61.-k, 82.45.-h, 87.16.Uv

I. INTRODUCTION

Motion of micrometer-sized swimmers, directly driven by an inhomogeneous chemical surface reaction, has recently attracted much scientific interest. While the mechanism was originally suggested as a mode of biological self-propulsion^{1,2}, currently studied swimmers are mostly artificial. A variety of systems featuring this chemical self-propulsion, have been investigated^{3,4}. The employed reactions often involve hydrogen peroxide which decomposes on the metal⁵⁻⁹ or enzyme-coated¹⁰ surfaces of the swimmers. Other mechanisms are, e.g., oxidation and reduction of glucose¹¹, hydrolyzation¹² or bromination¹³ at droplet surfaces, and thermally induced phase separation around a swimmer¹⁴. Finally, a number of theoretical studies have been conducted with generic chemical reaction schemes¹⁵⁻¹⁷. In previous theoretical work^{18,19} we have investigated the efficiency of this surface-driven propulsion since its exciting potential for use with micro-machines has been amply demonstrated²⁰⁻²³. Chemically driven microswimmers can also be used as model systems to investigate the physical principles of non-equilibrium diffusive motion²⁴⁻²⁶. Mutual interactions²⁷⁻³⁰ and the influence of confinement on the swimming³¹⁻³³ are a further active field of research.

A number of physical driving mechanisms for hydrogen peroxide based propulsion have been suggested. One of them is diffusiophoresis, which is particle motion through its interaction with a concentration gradient^{15,34,35}. An alternative, that is seen to dominate for large-scale swimmers, is the recoil of oxygen bubbles^{36,37}. Pressure waves were also suggested as a possible origin of motion³⁸. Finally, it has been found that metallic microswimmers swim through self-electrophoresis^{39,40}. Self-electrophoresis is the swimming of a charged particle through electric interaction with a self-generated, charged environment.

The work in this article is motivated by the experiments with metallic swimmers done by Sen, Mal-

loux, Wang and co-workers^{39,40} following their work with Paxton et al.⁴¹. There, bimetallic microrods (often a platinum-gold particle) were immersed in an hydrogen peroxide (H_2O_2) solution. The surface of the rods catalyzes a decomposition of H_2O_2 into oxygen $O_2(g)$ and water. It has been found that the mechanism for electrokinetic decomposition of H_2O_2 involves an electric current inside the microrod, which causes a concentration gradient of ions in the fluid surrounding the swimmer. Since the rod interacts through an electric potential with the ions, a gradient of the latter leads to swimming. The swimming speed increases linearly with the concentration of H_2O_2 until it saturates above concentrations of about 5%. An interpretation of this saturation has been given in the framework of a Michaelis-Menten-like surface kinetics. Wang et al.⁴⁰ conducted a comprehensive study using different combinations of metals for bimetallic microswimmers. A clear correlation between the mixed potential difference between the two metals and the swimming speed was found. By choice of optimal materials⁴² for the anode, cathode and intermediate part of the swimmer, the speed could even be increased to more than $50 \mu\text{m/s}$. In order to understand the electrokinetic driving mechanism quantitatively, a few theoretical studies have been conducted. Sundararajan et al.⁴³ compared experimental data with a numerical model where the rate of the cation exchange was fixed. Yariv⁴⁴ conducted a thorough study of the case of a thin diffuse layer of charges surrounding the particle. His linear response theory included surface reaction kinetics explicitly. Moran and Posner⁴⁵ investigated a full numerical model for rather thick, diffuse layers of ions around the swimmer. Most recently, they included a surface reaction that is second order in H^+ concentration⁴⁶. This work provided a closed, quantitative model that could be directly compared to experimental data. Their results indicated a quadratic increase of the swimming speed with the concentration of H_2O_2 , which, however, is not observed in the experiment. Building on the work described

above, we here investigate a complementary, non-linear model for a charged double layer structure that is much thinner than the radius of the swimmer.

An estimate of the ion concentrations³⁹ around the swimmers suggests that these systems are operating quite far away from equilibrium. On the other hand, the linear speed vs. concentration relation at low and moderate H_2O_2 concentrations does hint that a theory containing linear response elements may still be valid. Therefore, we choose a combination of numerical modeling and analytical approximation to capture the non-equilibrium behavior of the system and provide simple explanations for qualitative trends.

Any model of self-electrophoretic swimming is hampered by a general lack of knowledge concerning the complex details of the surface reaction mechanism. In particular, the dependence of surface charge accumulation on the reaction rate is largely unknown. Since the electric potential of the swimmer directly influences its swimming speed, a better understanding of the effect of charge screening and ion adsorption is highly desirable. To pave the way for further investigations of these problems we model the system as simple as possible, demonstrating only the generic aspects.

II. THE MODEL

A. Swimmer in an ionic solution

We employ the commonly used hydrodynamic model for electrophoretic effects⁴⁷. Throughout this publication, we will designate dimensional variables with a tilde ($\tilde{}$). Dimensional constants are written in calligraphic letters. The swimmer, a spherical particle with radius \mathcal{R} , is placed in an infinitely large container (Fig. 1). Swimming speed will be denoted by \tilde{U} . The fluid surrounding the particle is assumed to be incompressible and Newtonian with a constant viscosity η . Mass flow velocity is denoted by $\tilde{\mathbf{v}}$. The fluid contains ions that carry only one unit charge each. The concentrations of salt anions and cations in the solution are denoted by \tilde{c}^{i-} and \tilde{c}^{i+} , respectively. The hydroxide (OH^-) and proton (H^+) concentrations, resulting from the spontaneous dissociation of water and from the electrocatalytic process, are denoted by \tilde{c}^{H-} and \tilde{c}^{H+} , respectively. All types of ions are assumed to have the same diffusion constant \mathcal{D} . Concentrations of cations and anions are denoted summarily by

$$\begin{aligned}\tilde{c}^+ &\equiv \tilde{c}^{H+} + \tilde{c}^{i+}, \\ \tilde{c}^- &\equiv \tilde{c}^{H-} + \tilde{c}^{i-}.\end{aligned}\quad (1)$$

The ions couple to an electric field $\tilde{\phi}$. In the bulk, far away from the swimmer, we have charge neutrality and the concentrations of ions are equal $\tilde{c}^-(\infty) = \tilde{c}^+(\infty)$. The swimmer is axially symmetric. Therefore we use a spherical coordinate system aligned in the $\hat{\mathbf{e}}_z$ direction,

where \tilde{r} is the distance from the particle center and ϑ is the inclination angle. The unit vectors of the spherical system are denoted by $\hat{\mathbf{e}}_r, \hat{\mathbf{e}}_\vartheta$.

We non-dimensionalize length with the swimmer radius \mathcal{R} and the concentrations of ions \tilde{c}^\pm with the bulk concentration of salt ions $\mathcal{C} = \tilde{c}^{i+}(\infty) = \tilde{c}^{i-}(\infty)$. Energies are normalized with the thermal energy scale $k_b\mathcal{T}$. Accordingly, the electric potential $\tilde{\phi}$ is made non-dimensional with the thermal voltage $k_b\mathcal{T}/Ze \simeq 25$ mV. Throughout the publication we set $Z = 1$. Diffusive fluxes are non-dimensionalized with $\mathcal{D}\mathcal{C}/\mathcal{R}$. The velocity scale of the flow $\tilde{\mathbf{v}}$ and the swimming speed \tilde{U} is given by a typical speed \mathcal{U} . The Peclet number associated with transport of cations and anions is given by $Pe \equiv \mathcal{U}\mathcal{R}/\mathcal{D}$.

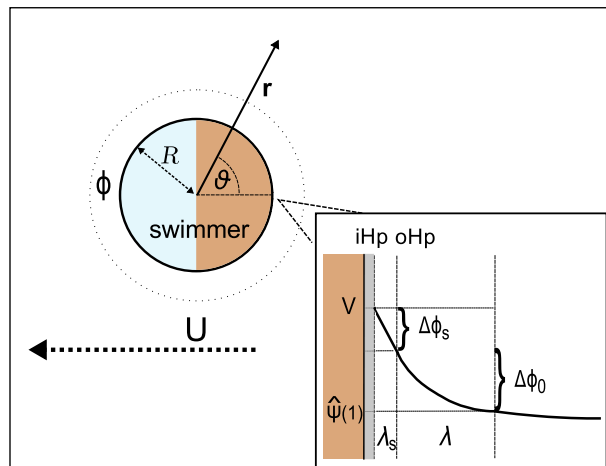


FIG. 1. Schematic representation of the model for a self-electrophoretic swimmer with radius \mathcal{R} moving with swimming speed U . The electric potential outside the swimmer is denoted by ϕ . The inset shows an enlarged version of our double layer model. The swimmer surface is covered by an immobile, compact layer of salt ions, termed Stern layer. The inner Helmholtz plane (iHp) and outer Helmholtz plane (oHp) delimit the modeled region of the Stern layer with thickness λ_s . Bordering to the outer Helmholtz plane we have the diffuse layer, where dilute solutes form a charge cloud around the swimmer. The diffuse layer has a thickness λ .

B. Poisson-Boltzmann and diffusion equations

The fluxes of cations and anions are given in dimensionless form by

$$\mathbf{j}^{\{H,i\},+} = -\nabla c^{\{H,i\},+} - c^{\{H,i\},+} \nabla \phi + Pe \mathbf{v} c^{\{H,i\},+}, \quad (2)$$

$$\mathbf{j}^{\{H,i\},-} = -\nabla c^{\{H,i\},-} + c^{\{H,i\},-} \nabla \phi + Pe \mathbf{v} c^{\{H,i\},-}. \quad (3)$$

Diffusion equations guarantee the conservation of substance in the fluid. They determine the concentration

field and read

$$\nabla \cdot \mathbf{j}^{\{H,i\},+} = 0, \quad (4)$$

$$\nabla \cdot \mathbf{j}^{\{H,i\},-} = 0. \quad (5)$$

The Poisson-Boltzmann equation provides a connection between the ion density and the electric field. It reads in dimensionless form

$$\nabla^2 \phi = -\frac{1}{2\lambda^2}(c^+ - c^-). \quad (6)$$

The lengthscale of the potential ϕ in Eq. (6) is given by the dimensionless Debye length λ , which we define as

$$\lambda \equiv \sqrt{\frac{\epsilon k_b \mathcal{T}}{8\pi e^2 \mathcal{N}_A \mathcal{C}}} \frac{1}{\mathcal{R}} \quad (7)$$

with \mathcal{N}_A being the Avogadro constant and ϵ the permittivity of the solution.

C. Stern layer and boundary conditions

In the bulk, far away from the swimmer, the electric potential takes on a uniform value which we set to zero

$$\phi(r \rightarrow \infty, \vartheta) = 0. \quad (8)$$

The presence of salt in the solution suggests some form of adsorption of ions onto the metal surface. The inset of Fig. 1 illustrates the employed model of a Stern (compact)-layer of immobile ions covering the metal surface⁴⁸. All the charge in the Stern layer is assumed to be concentrated in one plane, called inner Helmholtz plane (iHp). This plane almost coincides with the metal surface. We do not consider the details of the structure beyond the inner Helmholtz plane. The boundary between the Stern layer and the diffuse layer is termed outer Helmholtz plane (oHp). The voltage difference between inner and outer Helmholtz plane is called Stern layer voltage drop $\Delta\phi_s(\vartheta)$. The electric potential at the inner Helmholtz plane V equals $\Delta\phi_s(\vartheta)$ plus the change of the potential between outer Helmholtz plane and infinity $\phi(1, \vartheta)$:

$$V = \Delta\phi_s(\vartheta) + \phi(1, \vartheta). \quad (9)$$

Since we have an electric current flowing through the swimmer, the potential V may not be strictly constant. However, the electric conductivity of the metal swimmer is much higher than the conductivity of the surrounding solution. We therefore assume that the variation of V is negligible. *A priori*, the potential change over the Stern layer, $\Delta\phi_s(\vartheta)$, is unknown. If it depends on the potential right outside the immobile layer, it becomes ϑ -dependent. Since one postulates that the Stern layer outside the inner Helmholtz plane is charge free, Gauss's law can be employed to arrive at

$$\Delta\phi_s(\vartheta) = -\lambda_s \frac{\partial\phi(r, \vartheta)}{\partial r} \Big|_{r=1}, \quad (10)$$

where the parameter λ_s is the dimensionless thickness of the Stern layer between inner and outer Helmholtz plane.

The electrocatalytic process leading to a decomposition of H_2O_2 is supposed to take place at the inner Helmholtz plane. It leads to an absorption and emission of H^+ ions with a rate $\alpha(\vartheta)$, non-dimensionalized with the flux $\mathcal{C}\mathcal{D}/\mathcal{R}$. Boundary conditions, determining the concentrations of ions, result as

$$\hat{\mathbf{e}}_r \mathbf{j}^{H,+}(1, \vartheta) = \alpha(\vartheta), \quad (11)$$

$$\hat{\mathbf{e}}_r \mathbf{j}^{i,\pm}(1, \vartheta) = \hat{\mathbf{e}}_r \mathbf{j}^{H,-}(1, \vartheta) = 0, \quad (12)$$

$$c^{i,\pm}(r \rightarrow \infty, \vartheta) = 1, \quad (13)$$

$$c^{H,\pm}(r \rightarrow \infty, \vartheta) = \delta. \quad (14)$$

The constant δ is the relative concentration of H^+ ions in the bulk. It is defined by

$$\delta \equiv \tilde{c}^{H,+}(\infty)/\mathcal{C}. \quad (15)$$

In order to keep the charge of the swimmer constant the exchange of cations at its surface must satisfy

$$\int \hat{\mathbf{e}}_r \mathbf{j}^{H,+}(1, \vartheta) dA_{r=1} = 0. \quad (16)$$

D. Hydrodynamic equations

The mass flow velocity \mathbf{v} is determined by the Stokes equation for overdamped motion

$$\nabla \cdot \sigma = \nabla^2 \mathbf{v} - \nabla p = g(c^+ - c^-) \nabla \phi \quad (17)$$

where p is the pressure and $\sigma \equiv \nabla \mathbf{v} + (\nabla \mathbf{v})^T - p\mathbf{I}$ is the hydrodynamic stress tensor. We have also defined the non-dimensional constant

$$g \equiv \frac{\mathcal{R}\mathcal{C}k_b\mathcal{T}}{\eta\mathcal{U}}. \quad (18)$$

The boundary conditions on the fluid flow are

$$\mathbf{v}(r \rightarrow \infty, \vartheta) = \mathbf{U}, \quad (19)$$

$$\mathbf{v}(0, \vartheta) = 0, \quad (20)$$

where the swimming velocity \mathbf{U} is calculated from the balance of forces on the particle

$$0 = \int g(c^+ - c^-) \nabla \phi dV + \int \sigma \hat{\mathbf{e}}_r dA_{r=1}. \quad (21)$$

For a body force $g(c^+ - c^-) \nabla \phi$ that is independent of the fluid velocity \mathbf{v} one can employ Teubner's formula⁴⁹ to calculate the swimming speed as

$$U = -\frac{g}{6\pi} \int \left[\left(\frac{3}{2r} - \frac{1}{2r^3} - 1 \right) \cos \vartheta (c^+ - c^-) \partial_r \phi - \left(\frac{3}{4r} + \frac{1}{4r^3} - 1 \right) \sin \vartheta (c^+ - c^-) \frac{\partial_\vartheta \phi}{r} \right] dV. \quad (22)$$

E. Redox reactions at the surface of the swimmer

The electrochemical reactions leading to the decomposition of H_2O_2 at the swimmer's surface are complicated, especially since a number of inhibitory processes are involved. Experimental evidence supports the view that the reaction rate depends non-linearly on the H_2O_2 concentrations^{6,8}, most visibly for $c_{H_2O_2} \gtrsim 5\%$. The inferred (Michaelis-Menten-like) kinetics for a microswimmer agrees with other findings⁵⁰. This kinetics is probably due to saturation of active sites at the surface. Here we do not model the saturation but focus on low concentrations of educts and products. Experiments with comparatively large (mm-sized) electrodes suggest that the decomposition of hydrogen-peroxide at metal surfaces in acidic medium happens via a formation of oxides at the surfaces⁵¹. As also discussed in App. A, this intermediate may serve to justify an effective description in terms of a first order surface reaction. Fig. 2 illustrates that protons combine with H_2O_2 for the reduction of H_2O_2 . Therefore, the rate of H^+ consumption is assumed to be $\sim c^{H,+}(1, \vartheta) c_{H_2O_2}$. Electrocatalytic oxidation is supposed to supply the protons with a rate proportional to $c_{H_2O_2}$.

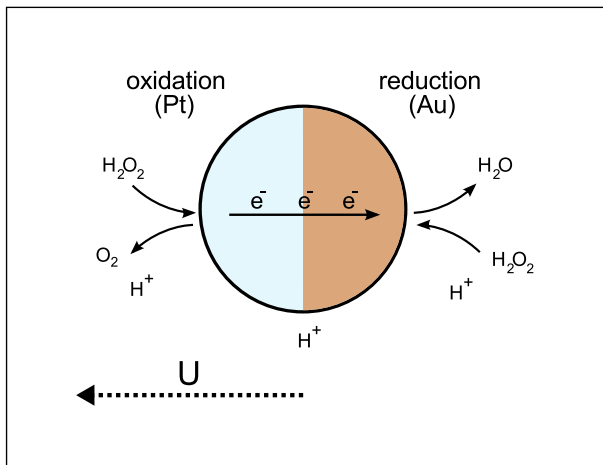


FIG. 2. Sketch of the electrokinetic process taking place at the swimmer's surface as described in Sec. II E. Note that the swimmer is found to move with the oxidizing end forwards.

The redox reactions at the swimmer's surface cause proton fluxes and involve a charge transfer. Therefore, the electric potential influences the reaction rate. We model this dependence with the established Butler-Volmer kinetics⁵²⁻⁵⁴. It is assumed that the reaction takes place at the inner Helmholtz plane, almost coinciding with the metal surface of the swimmer (see Fig. 1). Since the Stern layer is only described in an effective way, the energetic cost of passing from the outer to the inner Helmholtz plane must be incorporated explicitly into the reaction rates. This is commonly done by introducing rates that depend exponentially on $\Delta\phi_s(\vartheta)$ and

satisfy detailed balance. We choose rates $\sim e^{\pm \frac{\Delta\phi_s(\vartheta)}{2}}$, where the transfer coefficient, modifying $\Delta\phi_s$ in the exponents, is set to 1/2. For simplicity, we neglect further direct effects of the compact salt layer, that could, e.g., reduce the catalytic activity by covering the active sites. Evidently, ϕ also modifies the reaction rate by influencing the concentration of protons right outside the Stern layer $c^{H,+}(1, \vartheta)$. This dependence is however implicit and it does not appear in the rate equation. The overall rate of proton exchange at the swimmer's surface takes the form

$$\alpha(\vartheta) = - (K_1 + k_1 \cos \vartheta) e^{-\frac{\Delta\phi_s(\vartheta)}{2}} c^{H,+}(1, \vartheta) c_{H_2O_2} + (K_2 - k_2 \cos \vartheta) e^{\frac{\Delta\phi_s(\vartheta)}{2}} c_{H_2O_2}, \quad (23)$$

with $K_1 \geq k_1$ and $K_2 \geq k_2$. The first term in Eq. (23) models the catalytic reduction of H_2O_2 while the second term models the provision of H^+ ions through an oxidation. The constants k_1 and k_2 reflect the difference of redox potentials between the two metals composing the swimmer. Note that the linear dependence of $\alpha(\vartheta)$ on the H_2O_2 concentration in the bulk merely rescales all rate constants in the same way. The bulk concentration of H_2O_2 is a model parameter. We choose to express $c_{H_2O_2}$ in (dimensionless) fractions of 1% wt/v in order to facilitate the comparison with experimental data. In not modeling the H_2O_2 concentration explicitly we have assumed that a diffusive supply of this reagent is not the bottleneck of the reaction mechanism and that the encounter of H_2O_2 with the surface can be incorporated in the effective rate constants.

III. THEORY FOR THIN DIFFUSE LAYERS

If the Debye length is small, one can attempt an expansion of the concentration and potential fields in orders of λ , which largely simplifies the nonlinear equations. We follow here the classical approach outlined, e.g. by Hunter⁵⁵ which was used recently in the group of Bazant^{53,56} to model time dependent electrochemical processes.

A. The nonlinear problem

The technical details of the nonlinear double layer model are lengthy. We therefore defer them to App. B. Here we only sketch the mathematical procedure and present the result for the swimming speed. The field variables are expanded in powers of λ as

$$\begin{aligned} c^{i,\pm} &= c_0^{i,\pm} + \lambda c_1^{i,\pm} + \dots, \\ c^{H,\pm} &= c_0^{H,\pm} + \lambda c_1^{H,\pm} + \dots, \\ \phi &= \phi_0 + \lambda \phi_1 + \dots \end{aligned} \quad (24)$$

In the following, we only consider the terms of lowest order, $O(\lambda^0)$. The strategy is now to solve the non-linear

field equations both in an outer region, far away from the surface, and inside the diffuse layer. The inner and outer solutions are then matched to each other, such that a uniformly valid solution can be constructed. We distinguish the outer variables from the inner ones through a hat ($\hat{\cdot}$) on the former. Also, the potential ϕ_0 is written as sum of an inner and outer solution

$$\phi_0 = \psi_0 + \hat{\psi}_0. \quad (25)$$

The quasi one-dimensional equations for the inner variables can be solved analytically while the outer equations must be solved numerically. The result for the electric potential in the diffuse layer is

$$\begin{aligned} \phi_0(y, \vartheta) = \psi_0(y, \vartheta) + \hat{\psi}_0(1, \vartheta) = \\ 2 \ln \left[\frac{1 + \gamma(\vartheta)e^{-\sqrt{B(\vartheta)y}}}{1 - \gamma(\vartheta)e^{-\sqrt{B(\vartheta)y}}} \right] + \hat{\psi}_0(1, \vartheta), \end{aligned} \quad (26)$$

where we defined $y \equiv (r - 1)/\lambda$. The function $\gamma(\vartheta)$ is determined by the boundary conditions on the swimmer surface (see App. B). $B(\vartheta)$ is proportional to the overall concentration of ions at the outer boundary of the diffuse layer

$$B(\vartheta) \equiv \left(\hat{c}_0^{H,+}(1, \vartheta) + \hat{c}_0^{H,-}(1, \vartheta) + \hat{c}_0^{i,+}(1, \vartheta) + \hat{c}_0^{i,-}(1, \vartheta) \right) / 2. \quad (27)$$

Given (numerical) solutions for $\hat{\psi}_0$ and the potential at the swimmer surface V_0 , we can use Eq. (9) to calculate the potential drop across the diffuse layer $\Delta\phi_0(\vartheta)$ as

$$\Delta\phi_0(\vartheta) = V_0 - \Delta\phi_s(\vartheta) - \hat{\psi}_0(1, \vartheta), \quad (28)$$

where the voltage drop across the Stern layer $\Delta\phi_s(\vartheta)$ is calculated through Eq. (10). $\Delta\phi_0(\vartheta)$ can be interpreted as an angle-dependent zeta potential. The final result for the swimming speed reads, in terms of the above defined variables,

$$\begin{aligned} U \approx U_0 = g\lambda^2 \int_0^\pi [\Delta\phi_0(\vartheta) \frac{\partial \hat{\psi}_0(1, \vartheta)}{\partial \vartheta} \sin^2(\vartheta) - \\ 4 \ln \left(\cosh \left(\frac{\Delta\phi_0(\vartheta)}{4} \right) \right) \frac{\partial \ln(B(\vartheta))}{\partial \vartheta} \sin^2(\vartheta)] d\vartheta. \end{aligned} \quad (29)$$

We will omit the index at U_0 in the following since we do not deal with higher orders in λ . Remarkably, Eq. (29) has the same form as the celebrated formula by Dukhin and Derjaguin^{34,57}, which was derived for the linear response regime. The only difference is that the potential drop across the diffuse layer can not be approximated by the equilibrium zeta potential and is now ϑ -dependent. The dependence of U on $\Delta\phi_0$ allows to separate electrophoretic and diffusiophoretic contributions in the lowest order swimming speed⁵⁸. The first term in the integrand of Eq. (29) changes sign with $\Delta\phi_0$, similar to electrophoresis, where the particle swimming is also

reversed with the sign of the zeta potential. Therefore, the first term can be interpreted as the electrophoretic part. The second term does not change sign with the potential $\Delta\phi_0$ since $-4 \ln(\cosh(\Delta\phi_0/4)) = 2 \ln(1 - \gamma^2)$ is negative semi-definite. Its dependence on a gradient in overall concentration suggests an interpretation of the second term as diffusiophoretic contribution.

B. Analytical approximation

We assume now that the redox potential difference between the two sides of the swimmer is considerably smaller than its overall redox potential. This case can be modeled by setting $K_1, K_2 \gg k_1, k_2$. In a steady state, the constant H_2O_2 decomposition will modify the electric charge of the swimmer. If, additionally, k_1 and k_2 are neglected, no net cation flux can take place since a radially symmetric flux violates the charge conservation. The concentration of protons near the surface then follows a Boltzmann distribution $\sim \delta \exp[-\phi_{0,0}(y)]$, where the second index 0, here at $\phi_{0,0}$, indicates that we are considering the solution of order (k_1^0, k_2^0) . In this limit, Eq. (23) becomes

$$0 = -K_1 e^{-\frac{\Delta\phi_{s,0}}{2}} \delta e^{-\phi_{0,0}(0)} c_{H_2O_2} + K_2 e^{\frac{\Delta\phi_{s,0}}{2}} c_{H_2O_2}, \quad (30)$$

It follows that the swimmer's potential in steady state

$$V_{0,0} \equiv \Delta\phi_{s,0} + \phi_{0,0}(0) = \ln(K_1 \delta / K_2) \quad (31)$$

does not depend explicitly on the H_2O_2 concentration to lowest order. The swimming speed is calculated in App. C. We find

$$U \approx g\lambda^2 \frac{2 \ln(1 + \gamma_0)}{1 + \delta} \int \alpha_{0,1} \cos \vartheta d \cos \vartheta \quad (32)$$

where the integral is a measure of the dipole moment of the first order H^+ emission/absorption rate $\alpha_{0,1}$. We also defined $\gamma_0 \equiv \tanh(\phi_{0,0}(0)/4)$. Eq. (32) is similar to previously derived linear response formulas⁴⁴. When inserting $\alpha_{0,1}$, which is calculated in App. C, we have

$$U \approx g\lambda^2 \frac{8 \ln(1 + \gamma_0)}{3} \frac{\delta \left(k_2 + k_1 \frac{K_2}{K_1} \right) c_{H_2O_2}}{2\delta e^{-\frac{\Delta\phi_{s,0}}{2}} + K_2 c_{H_2O_2}}. \quad (33)$$

For a weak potential outside the compact layer, $\phi_{0,0} \lesssim 1$, one can estimate the dependence of the swimming speed on the particle potential through $\ln(1 + \gamma_0) \simeq (V_0 - \Delta\phi_{s,0})/4$.

IV. NUMERICAL VALUES FOR THE MODEL CONSTANTS

The thermal energy scale is $k_b \mathcal{T} = 4.11 \times 10^{-21}$ J. For the solution viscosity, we choose $\eta = 9 \times 10^{-4}$ Pa.s. For

the permittivity of the solution around the swimmer, we choose $\epsilon = 80 \epsilon_{vak}$. Typically, the experimental swimmers have lengths in the 300 nm - 5 μm range. We set the radius of our swimmer to

$$\mathcal{R} \equiv 1 \mu\text{m}. \quad (34)$$

A velocity scale can be defined, which is independent of the concentration scale. We set

$$\mathcal{U}g\lambda^2 = \frac{(k_b T)^2 \epsilon}{8\pi\eta e^2 \mathcal{R}} \simeq 20.6 \mu\text{m/s}. \quad (35)$$

In this work we rely on the addition of extra salt to the solution to explicitly justify the usage of the thin diffuse layer model. Where not explicitly mentioned otherwise, we set the bulk concentration of salt ions in the following to

$$\mathcal{C} = 5 \times 10^{-5} \text{ mol/L}. \quad (36)$$

For a monovalent salt, e.g., NaNNO_3 as used by Paxton et al.³⁹, according to Eq. (7), we have a thickness of the diffuse layer of $\simeq 12 \text{ nm}$. Since this is much smaller than $\mathcal{R} = 1 \mu\text{m}$ our theory for $\lambda \ll 1$ is expected to work well. The absolute thickness of the Stern layer is usually assumed to be in the order of a molecular diameter⁵⁹, which might be about 0.3 nm .

For propulsion of our microswimmers we consider a $[10^{-4} \dots 5] \%$ solution of H_2O_2 in water. Percent of H_2O_2 concentration are given in wt/v (1 % wt/v corresponds to 10g H_2O_2 per liter solvent, molar mass of H_2O_2 : 34.02 g/mol). The pH value decreases here almost linearly with an increase of H_2O_2 concentration⁶⁰. It lies roughly between 7 and 5. This sets the concentration of bulk protons and hydroxide ions to $\tilde{c}^{H,\pm}(\infty) \simeq [10^{-7} \dots 10^{-5}] \text{ mol/L}$. The relative concentration of H^+ ions in the bulk is then in the range $\delta = \tilde{c}^H(\infty)/\mathcal{C} \simeq [10^{-3} \dots 10^{-1}]$.

For the diffusion constant, we choose $\mathcal{D} = 7 \times 10^{-9} \text{ m}^2/\text{s}$. The ion fluxes at the surface are then non-dimensionalized with

$$\mathcal{C}\mathcal{D}/\mathcal{R} = 3.5 \times 10^{-4} \text{ mol/m}^2 \text{ s}. \quad (37)$$

A measured³⁹ evolution rate of O_2 for a 3.7 % solution of H_2O_2 is $8.7 \times 10^{-6} \text{ mol/m}^2 \text{ s}$. Within our reaction model, Eq. (23), this rate roughly determines the magnitude of the second term, responsible for the oxidation of H_2O_2 . For $c_{\text{H}_2\text{O}_2} = 1$ (1 %) we estimate that $K_2 c_{\text{H}_2\text{O}_2}$ is on the order of 10^{-2} . We assume that its value scales linearly in the range of employed H_2O_2 solutions. The constants K_1, k_1, k_2 are chosen such that we obtain reasonable values for the swimming speed and the proton fluxes.

V. RESULTS

In order to facilitate a comparison with experimental data, we often display dimensional quantities in the

following. The dimensional speed is calculated as $\tilde{U} = \mathcal{U}U = 20.6 \mu\text{m/s} \times U/(g\lambda^2)$. Results for the analytical approximation of U (Eq. (33)) are also shown where applicable.

A. Reaction induced concentration distortion

Fig. 3 shows exemplary concentration fields of positive ions around the swimmer. While the concentrations of H^+ in Figs. 3 a,c are directly determined through the surface reactions, the inhomogeneous distribution of positive salt ions seen in Figs. 3 b,d is an indirect effect. The positive salt ions accumulate oppositely to the H^+ ions. They present a non-negligible contribution to the local charge balance. In Figs. 3 a,b we have $(k_1, k_2) \ll (K_1, K_2)$, i.e., the decomposition of H_2O_2 happens fairly homogeneously around the swimmer. In this case the concentration profile is antisymmetric and follows the distribution of surface reactivity. In Figs. 3 c,d we have set $k_1 = K_1$ and $k_2 = K_2$, i.e., the reaction happens mainly in an asymmetric way, where oxidation and reduction take place on different sides of the swimmer. Also, the concentration of H^+ ions in the bulk is not assumed to be excessive. Then the concentration variation around the swimmer feeds back on the overall reaction rate, Eq. (23). Consequently, the antisymmetric distribution of the cations seen in Figs. 3 a,b is lost. This reaction induced concentration distortion is a direct consequence of the usage of the mass action law to model the surface reaction. In our previous work we have found that it is important for the calculation of the swimming speed¹⁹.

B. Swimming and H_2O_2 concentration, fixed pH

Fig. 4 demonstrates the dependence of the swimming speed \tilde{U} on the concentration of H_2O_2 with a fixed pH value. A fixed pH value means that the availability of H^+ in the bulk, determined by δ , does not change with H_2O_2 concentration. Eq. (33) approximates the numerically calculated swimming speed well for $k_1 < K_1$ and $k_2 < K_2$. However, the condition $k_2 < K_1$ for the validity of the analytical approximation seems here unnecessary.

The curves in Fig. (4) have a concave shape, which is not attributed to a saturation of the catalytic surface in our model. Rather, it results from a limitation of the reaction rate through the diffusion around the swimmer. Quantitative understanding of this effect can be gained from the approximative Eq. (33). Here we find a leveling off of the swimming speed since the rate of ion flux through the swimmer saturates for $K_2 c_{\text{H}_2\text{O}_2} \gtrsim 2\delta e^{-\frac{\Delta\phi_s,0}{2}}$. This estimate is seen to hold also for the results from the nonlinear numerics. A negative Stern layer voltage drop $\Delta\phi_s$ shifts the saturation of the speed to higher values of $c_{\text{H}_2\text{O}_2}$, while also reducing the speed (see Sec. V E). Figs. 5, 6 show how the average

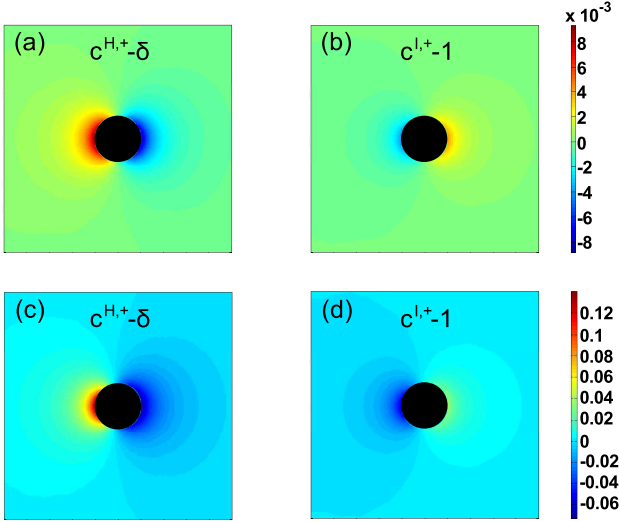


FIG. 3. Colorcoded concentrations of H^+ ions and positive salt ions. Figs. a,b and c,d each have the same color coding. $c_{H_2O_2} = 1$ (1%), $K_1 = 0.0185$, $K_2 = 0.185$, $\delta = 0.1$, and $\lambda_s = 0$. For Figs. a,b: $k_1 = 0.1 K_1$, $k_2 = 0.1 K_2$ resulting in $V_0 = -4.61$ and $U = -0.0398$. For Figs. c,d: $k_1 = K_1$, $k_2 = K_2$ resulting in $V_0 = -5.03$ and $U = -0.485$.

reaction rate $\langle |\alpha(\vartheta)| \rangle$ and the electric potential on the swimmer's surface V_0 change with the increase of H_2O_2 . Note that $\langle |\alpha(\vartheta)| \rangle$ can not be identified with the measurable oxygen evolution rate. $\langle |\alpha(\vartheta)| \rangle$ vanishes for equal redox potentials on both sides of the swimmer, i.e., if $k_1 = k_2 = 0$, while the oxygen evolution rate in this limit is, within our model, an unknown constant.

C. Swimming and H_2O_2 concentration, variable pH

Since the concentration of H_2O_2 also influences the pH value we plot in Fig. 7 the speed vs. $c_{H_2O_2}$ with H_2O_2 -dependent δ . The pH value decreases almost linearly with an increase of H_2O_2 concentration⁶⁰. Therefore we set $\delta = \delta_0 + \delta_1 c_{H_2O_2}$ where the dissociated water molecules at a pH value of 7 contribute $\delta_0 = (10^{-7} \text{ mol/L})/C$. The slope of the function is roughly estimated as $\delta_1 = 0.02$. The reaction rate is not expected to saturate here as seen from Eqns. (33,C20). The speed becomes an almost linear function of the H_2O_2 concentration. A remaining concave tendency of the functions is due to a reduction of the Debye length and a change of the particle potential with the pH value. The curves in Fig. 7 are very similar to what is measured experimentally^{6,42}.

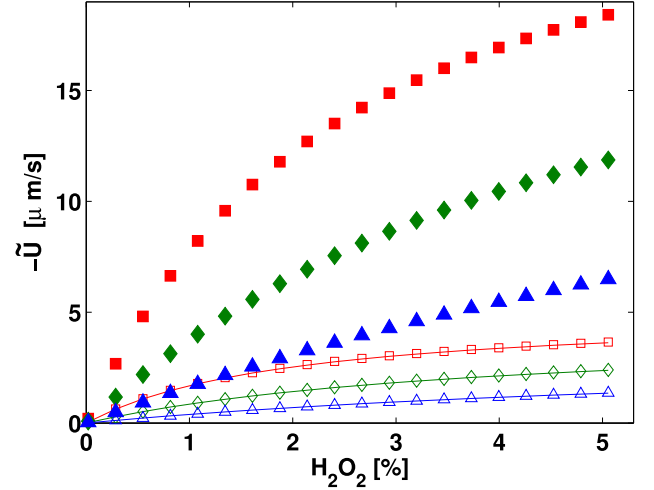


FIG. 4. Swimming speed \tilde{U} vs. H_2O_2 concentration at fixed pH value. $K_1 = 0.005$, $\delta = 0.1$, $\lambda_s = 0$. Symbols are numerical results. Full lines are approximative speeds from Eq. (33). (Red box): $K_2 = 0.1$, $k_2 = K_2$, $k_1 = K_1$. (Open red box): $K_2 = 0.1$, $k_2 = 0.25 K_2$, $k_1 = 0.25 K_1$. (Green diamond): $K_2 = 0.05$, $k_2 = K_2$, $k_1 = K_1$. (Open green diamond): $K_2 = 0.05$, $k_2 = 0.25 K_2$, $k_1 = 0.25 K_1$. (Blue triangle): $K_2 = 0.025$, $k_2 = K_2$, $k_1 = K_1$. (Open blue triangle): $K_2 = 0.025$, $k_2 = 0.25 K_2$, $k_1 = 0.25 K_1$.

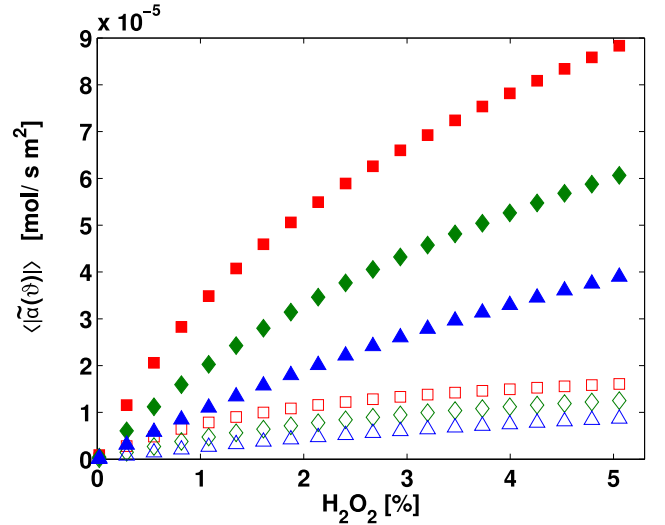


FIG. 5. Average ion current $\langle |\tilde{\alpha}(\vartheta)| \rangle$ vs. H_2O_2 concentration at fixed pH value. Symbols are the same as in Fig. 4.

D. Swimming and H_2O_2 reduction rate

In Fig. 8 we investigate the role of the rate constants of H_2O_2 reduction, K_1 and k_1 , for the swimming speed. We keep the quotient of K_1 and k_1 constant and Eq. (33) therefore suggests that the swimming speed is only

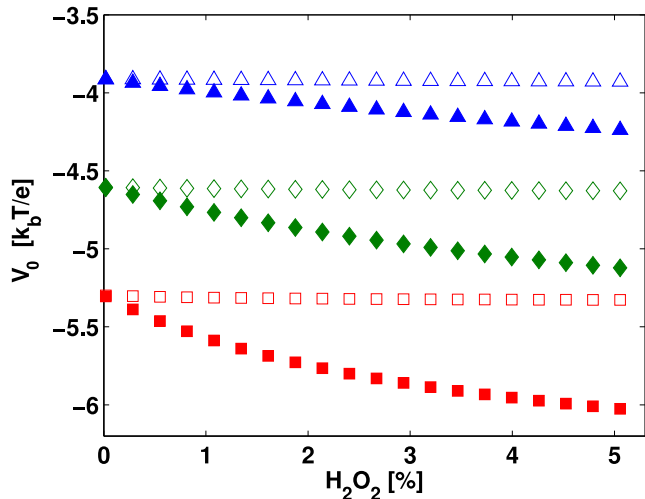


FIG. 6. Electric potential of the swimmer V_0 vs. H_2O_2 concentration at fixed pH value. Symbols are the same as in Fig. 4.

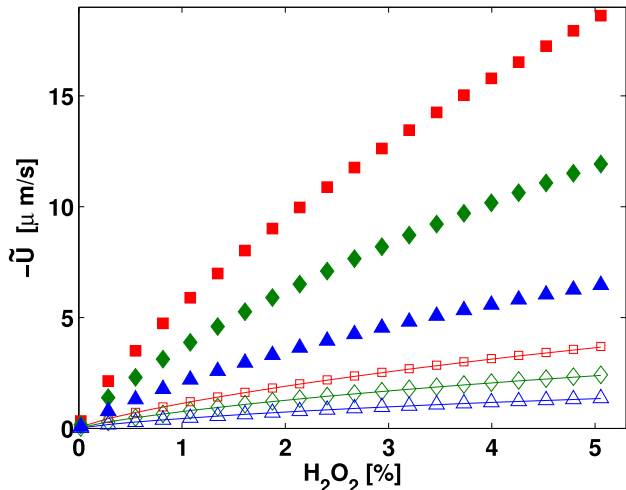


FIG. 7. Dependence of swimming speed \tilde{U} on H_2O_2 concentration where the pH value varies with $c_{H_2O_2}$. We use $\delta = 0.002 + 0.02 c_{H_2O_2}$. Symbols are the same as in Fig. 4.

influenced through its dependence on the particle potential V_0 via the function γ . The approximation for the swimmer's potential, Eq. (31), in turn suggests that V_0 depends logarithmically on $K_1\delta/K_2$. The numerical data qualitatively supports a scaling of \tilde{U} with this logarithm. The magnitude of the swimming speed is seen to decrease with an increase of K_1 . The negative sign of \tilde{U} is in accordance with the experimental finding that the swimming occurs in direction of the H_2O_2 -oxidizing end⁴⁰. However, for $K_1\delta > K_2$ we also find a reversion of the swimming direction, which results from the sign change

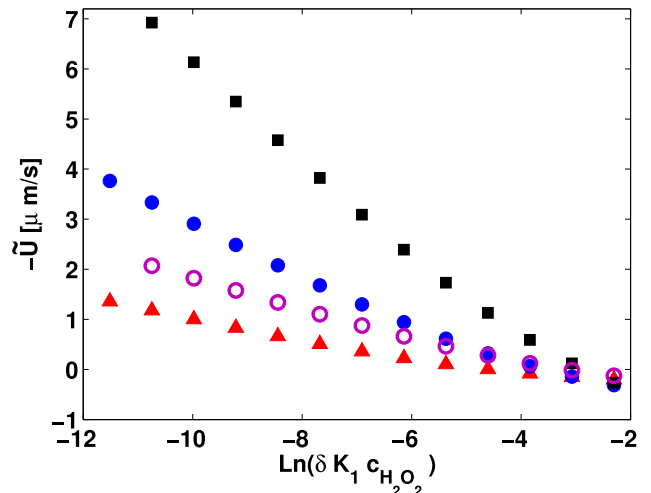


FIG. 8. Dependence of swimming speed \tilde{U} on the rate constant of H_2O_2 reduction K_1 at $c_{H_2O_2} = 1$ (1%) with $k_2 = K_2$, $k_1 = K_1$, and $\lambda_s = 0$. (Black box): $\delta = 0.1$, $K_2 = 0.05$. (Blue Dot): $\delta = 0.1$, $K_2 = 0.025$. (Violet circle): $\delta = 0.01$, $K_2 = 0.025$. (Red triangle): $\delta = 0.1$, $K_2 = 0.01$.

of V_0 .

E. Effect of the Stern layer

The Stern layer modifies the swimming speed for $V_0 < 0$ by reducing the reaction rate and the potential change in the diffuse layer, appearing in Eq. (29). Fig. 9 demonstrates that \tilde{U} decreases for our rate constants almost linearly with the average Stern layer voltage drop ($\Delta\phi_s(\vartheta)$). The approximation, Eq. (33), does not yield satisfactory absolute values for \tilde{U} in Fig. 9 since we have here $k_1 = K_1$ and $k_2 = K_2$. However, Eq. (33) can be expanded for small $\Delta\phi_s$. It then predicts the slopes of the decrease of \tilde{U} with $\Delta\phi_s$ fairly well. The inset of Fig. 9 demonstrates that $\Delta\phi_s$ depends non-linearly on the thickness of the layer λ_s/λ . This non-linear relationship occurs since the Stern layer voltage drop is determined through a transcendental equation (see appendix, Eq. (B30)).

The swimming speed scales within the thin diffuse layer model, Eq. (29), as the inverse of the overall bulk ion concentration $1/(C + C\delta)$. Experimental data supports this rough scaling, but also indicates deviations from it³⁹. One reason for a deviation may be the Stern layer, which influences the reaction rate. In our simple model, the connection between the Stern layer and the reaction is given through the appearance of $\Delta\phi_s$ in the Butler-Volmer Eq. (23). In a tempting first approximation, we here keep the absolute thickness of the Stern layer constant. The variations of the bulk salt concentration still affects the Stern layer voltage drop $\Delta\phi_s$ since $\lambda_s/\lambda \sim \sqrt{C}$. Fig. (10) demonstrates that this suffices

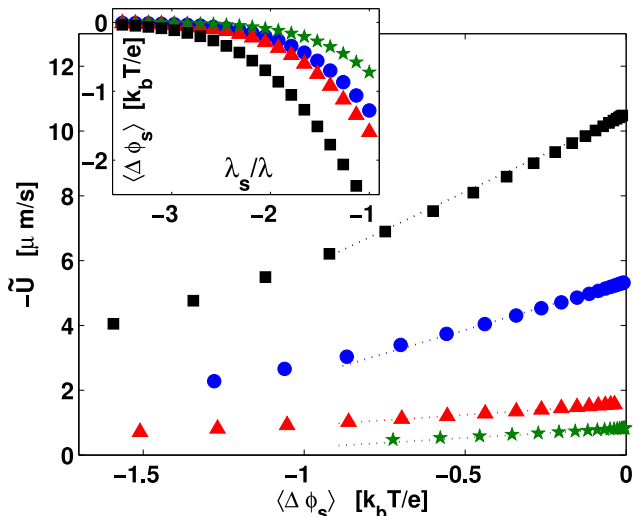


FIG. 9. Dependence of swimming speed \tilde{U} on the average Stern layer voltage drop $\langle \Delta \phi_s(\vartheta) \rangle$. Inset: dependence of $\langle \Delta \phi_s(\vartheta) \rangle$ on relative Stern layer thickness λ_s/λ . $c_{H_2O_2} = 1$ (1%) with $k_2 = K_2$, $k_1 = K_1$. (Black box): $\delta = 0.1$, $K_1 = 0.001$, $K_2 = 0.1$. (Blue Dot): $\delta = 0.1$, $K_1 = 0.001$, $K_2 = 0.05$. (Green star): $\delta = 0.1$, $K_1 = 0.001$, $K_2 = 0.01$. (Red triangle): $\delta = 0.01$, $K_1 = 10^{-4}$; $K_2 = 0.01$. (Dotted lines): slopes predicted by an expansion of Eq. (33) for small $\Delta \phi_s$.

to cause a reduction of the swimming speed compared with the standard scaling. A precise measurement of this effect, along with a more refined model of the ion adsorption is called for to improve the quantitative understanding here.

VI. DISCUSSION

Effects of salt on self-electrophoretic swimming become important when (bio-) technological applications are envisaged since physiologically or otherwise relevant environments are often ionic. One of these effects is the coupling of salt ion fluxes to the reaction-driven proton fluxes. In general, salt ions can not be described by a constant concentration background since this approximation causes non-negligible errors in the swimming speed. A full mathematical description leads to a system of non-linear equations, that must be solved numerically. We chose to focus on the thin diffuse layer approximation rather than solving the whole system of equations. The advantages of this approach are that the hydrodynamics become relatively simple and that a quite demanding high density of grid nodes near the surface can be avoided. The thin diffuse layer model may describe the swimming well, even in absence of electrolytes. Spontaneous dissociation of H_2O_2 in the bulk can be an important factor here. A reasonable pH value of 6 translates, e.g., to a double layer thickness, Eq. (7), of about 90 nm.

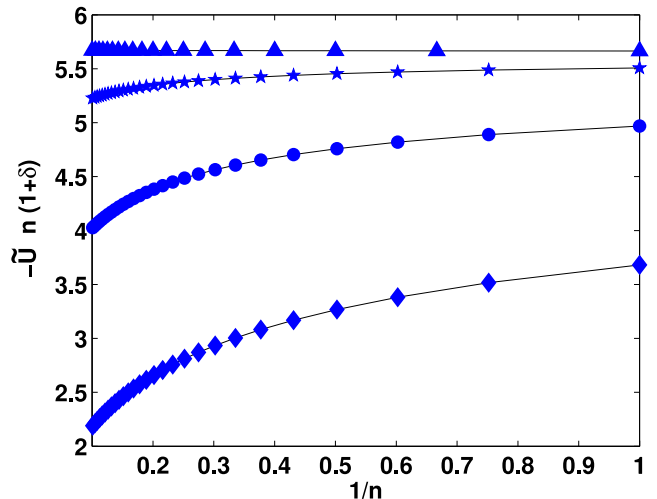


FIG. 10. Deviation of \tilde{U} from the standard thin diffuse layer scaling with the inverse ion concentration $\sim 1/(C + C\delta)$. Bulk salt concentrations are varied as $C = n \times (5 \times 10^{-5} \text{ mol/L})$ with $n = 1 \dots 10$. Speed is multiplied with $n(1 + \delta)$ to remove the standard scaling. $c_{H_2O_2} = 3.7$ (3.7%), $K_1 = k_1 = 0.005$, $K_2 = k_2 = 0.025/n$, $\delta = 0.1/n$. (Triangle): $\lambda_s/\lambda = 0$. (Star): $\lambda_s/\lambda = 0.005\sqrt{n}$. (Dot): $\lambda_s/\lambda = 0.025\sqrt{n}$. (Diamond): $\lambda_s/\lambda = 0.1\sqrt{n}$.

This number is an order of magnitude smaller than \mathcal{R} . It justifies the approximative use of the thin diffuse layer model for H_2O_2 concentrations, say, above the 2% range. A contamination of the water with atmospheric carbon dioxide has also been found to be important for electrophoresis in a salt-free environment⁶¹. The somewhat unknown details of the reaction mechanism at the surface of the swimmer could further contribute to making the thin diffuse layer model valid. It is, e.g., possible that the reactions at the swimmer's surface lead, beyond our model, to a further accumulation of other types of ions and radicals.

A new feature of our model is that we use first order Butler-Volmer kinetics for the electrocatalytic decomposition of H_2O_2 . This reaction leads to a linear increase of swimming speed at low H_2O_2 concentrations. The transport of protons around the swimmer can limit the reaction rate and therefore cause a saturation of the swimming speed at high H_2O_2 concentrations. We found that an expected decrease of the pH value with an increase of the H_2O_2 concentration can widely suppress the leveling off of the speed since the bulk H^+ ions take part in the catalytic reduction. Any other mechanism providing an excessive amount of H^+ ions would equally reduce the effect of proton diffusion and lead to a linear speed- $[H_2O_2]$ relation. The influence of proton transport on the reaction is not in conflict with an additional limitation of the rates though saturation of the catalytic surface in experimental systems.

The Butler-Volmer equation includes a further effect,

that is also related to the presence of salt: the Stern layer on the surface of the swimmer. In this article, we have undertaken a very first step towards an understanding of its influence on the swimming speed. The Stern layer lowers in our model the swimming speed by modifying the potential drop across the diffuse layer and by reducing the reaction rate. It is also responsible for a decrease of speed with increased salt concentration that is stronger than the inverse of the bulk ion concentration.

The swimmer's potential V plays an important role for the swimming speed since it is directly related to the potential drop across the diffuse layer (the zeta potential). For negligible Stern layers, V could possibly be determined experimentally by measuring the additional drift of actively swimming particles in an external field. In our model, we found V to be in most cases much lower than -40 mV, which is about the zeta potential of a metal particle without the presence of H_2O_2 . This value was used previously as a rough estimate⁶. Such a high potential V can only be found within our model if the overall oxidation and reduction rates are similar (see Eq. (31)).

In this article, we have made a few simplifying assumptions. First, we consider a spherical swimmer with a reactivity varying like a cosine across the surface. This geometry is chosen for its numerical robustness since no sharp edges and sudden changes are present. On the other hand, the experimentally studied swimmers are short, bimetallic rods where the reactivity varies quite suddenly across the boundary from one metal to the other. A second simplifying assumption is that all solutes have similar diffusivities. We guess that these simplifications together introduce a deviation from the experimental reference data by a factor of 1 – 5.

We have not modeled the adsorption of salt into the Stern layer explicitly but fixed its width at a molecular lengthscale. The influence ion adsorption on electrophoretic mobility is a long standing problem. A number of different models have been suggested to quantitatively account for different kinds of salt ions^{55,62}. The common assumption that the Stern layer is independent of salt concentration is somewhat justified for non-reactive, metallic interfaces⁶³ but remains an assumption for our system. Its validity may be particularly questioned once a variation of the salt concentration changes the reaction rate and thereby the swimmer's potential. Including an explicit adsorption mechanism is challenging. It would be desirable to have more experimental data concerning the interplay of salt and H_2O_2 decomposition at microswimmers before attempting such a model.

It is well known that double layers can exhibit lateral ion transport if they are highly charged⁶⁴. If contributions of the order $\lambda e^{-\Delta\phi_0/2}$ are not negligible, corrections to the λ^0 theory must incorporate electro-osmosis and electromigration in the diffuse layer. We have neglected the corrections due to these surface conduction phenomena in order to focus on the important trends of our model. An investigation of the role of surface transport for self-electrophoresis would be an important exten-

sion. A somewhat related topic is the possible occurrence of hydrodynamic slip on the surface of the swimmer. This slip might serve to enhance the swimming speed^{65,66}. Finally, the assumption of dilute solutes could be relaxed. However, non-electric interactions and the competition for catalytic binding sites would make an analytical description of solutes fairly complicated. Molecular dynamics simulations could offer a promising alternative here.

Taken together, our model quantitatively supports an explanation of the particle swimming in terms of self-electrophoresis^{39,40} and points to a number of interesting phenomena governing the details of this intriguing mode of micro-motion.

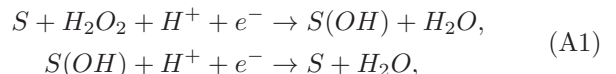
ACKNOWLEDGMENTS

We thank A. Sen, T.E. Mallouk and W.F. Paxton for useful comments.

Appendix A: Details of the redox reactions

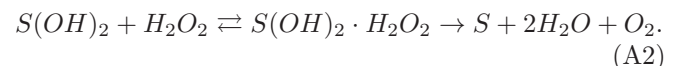
In this appendix, we illustrate the reaction rate postulated in Sec. II E with concrete, but simplified prototypical reaction pathways. We emphasize that the schemes discussed below merely present one possible way to justify the mathematical model we discuss in the main part. Due to the general lack of knowledge concerning the surface reactions, we can not claim that that these pathways are ultimately the dominant ones. However, preliminary studies with other rate equations made us confident that many qualitative trends presented above are quite robust.

During the reduction of H_2O_2 , H^+ ions in the vicinity of the metal surface combine with electrons form the metal substrate S . A possible scheme for this process is

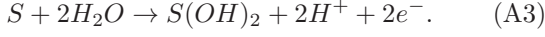


which has been used previously for a simulation of the reduction on platinum electrodes⁶⁷. Additional processes, that possibly slow down the reduction, are neglected here. We assume that the concentration of H_2O_2 is low, such that the availability of catalyst is not limiting. Applying the steady state condition, we find that the concentration of $S(OH)$ is independent of $[H^+]$. This implies that the effective rate equation for H^+ consumption is first order in $[H^+]$ and $[H_2O_2]$. A second order reaction rate can not be excluded, but we deem the suggested presence of a multi-step decomposition sufficient to allow the simpler modeling of the reduction as a first order process.

The oxidation of H_2O_2 at metal electrodes has been studied in great detail by Hall et al.^{50,68}. It is also found to depend on surface oxide films. A possible scheme for the reduction of the surface film is



Hydrogen ions are released when the surface is oxidized again



Neglecting side processes, one can again assume that the reaction is first order in $[H_2O_2]$. Four electron processes, as suggested by Wang et al.⁴⁰ are, for simplicity, not considered explicitly.

Appendix B: Nonlinear theory for $\lambda \rightarrow 0$

This appendix details the non-linear mathematical theory of a thin diffuse layer which is used in the main part of the article. We define new variables for the concentrations and expand them in powers of λ

$$\begin{aligned} m^{\{H,i\}} &\equiv c^{\{H,i\},+} - c^{\{H,i\},-} \\ &= m_0^{\{H,i\}} + \lambda m_1^{\{H,i\}} + \dots, \\ M^{\{H,i\}} &\equiv c^{\{H,i\},+} + c^{\{H,i\},-} \\ &= M_0^{\{H,i\}} + \lambda M_1^{\{H,i\}} + \dots, \\ \phi &= \phi_0 + \lambda \phi_1 + \dots \end{aligned} \quad (\text{B1})$$

Outer variables carry a hat (^), variables for the fields inside the diffuse layer do not carry a hat. The potential ϕ_0 is written as sum of an inner and outer solution

$$\phi_0 = \psi_0 + \hat{\psi}_0. \quad (\text{B2})$$

The equations determining the outer variables $\hat{M}_0^{\{H,i\}}$, $\hat{m}_0^{\{H,i\}}$ and $\hat{\psi}_0$ are written in terms of r and ϑ . The Poisson-Boltzmann equation (6) in the outer region reads with $\hat{m} \equiv \hat{m}^H + \hat{m}^i$

$$\nabla^2 \left(\hat{\psi}_0 + \lambda \hat{\psi}_1 \dots \right) = -\frac{1}{2\lambda^2} \left(\hat{m}_0 + \lambda \hat{m}_1 + \lambda^2 \hat{m}_2 \dots \right), \quad (\text{B3})$$

which is singular for $\lambda \rightarrow 0$ and therefore we require $\hat{m}_0 = \hat{m}_1 = 0$. This provides the condition of charge neutrality outside the diffuse layer. The number of lowest order outer variables is hence reduced by one

$$\hat{m}_0^H = -\hat{m}_0^i. \quad (\text{B4})$$

Note that the condition of charge neutrality does not require that the charges of the different ions balance individually. The relation $\hat{m}^H = \hat{m}^i = 0$ only holds in the bulk, far away from the particle. Concerning the singular behavior of Eq. (B3) we also mention that a charge of (vanishing) magnitude $\sim \lambda^2 \sim 1/\mathcal{C}$ results in a non-vanishing lowest order electric field in the outer region. Therefore, the electric potential can not be neglected in the diffusion equations, Eqns. (4,5), outside the diffuse layer. Eqns. (4,5) read to lowest order for the outer

region

$$\nabla \cdot \left(\nabla \hat{m}_0^H + \hat{M}_0^H \nabla \hat{\psi}_0 \right) = 0, \quad (\text{B5})$$

$$\nabla \cdot \left(-\nabla \hat{m}_0^H + \hat{M}_0^i \nabla \hat{\psi}_0 \right) = 0, \quad (\text{B6})$$

$$\nabla \cdot \left(\nabla \hat{M}_0^H + \hat{m}_0^H \nabla \hat{\psi}_0 \right) = 0, \quad (\text{B7})$$

$$\nabla \cdot \left(\nabla \hat{M}_0^i - \hat{m}_0^H \nabla \hat{\psi}_0 \right) = 0, \quad (\text{B8})$$

The convection terms do not appear in lowest order because the fluid velocity is $O(\lambda^2)$ (see below). The boundary conditions for $r \rightarrow \infty$ are given by the bulk concentration of ions as

$$\hat{M}_0^H(r \rightarrow \infty, \vartheta) = 2\delta, \quad (\text{B9})$$

$$\hat{M}_0^i(r \rightarrow \infty, \vartheta) = 2, \quad (\text{B10})$$

$$\hat{m}_0^H(r \rightarrow \infty, \vartheta) = 0, \quad (\text{B11})$$

$$\hat{\psi}_0(r \rightarrow \infty, \vartheta) = 0. \quad (\text{B12})$$

Near the surface we employ a stretched, radial coordinate $y \equiv (r-1)/\lambda$. The diffusion equations in the inner region are expanded up to $O(\lambda^0)$ and read

$$0 = -\partial_y \left(\partial_y m_0^{\{H,i\}} + M_0^{\{H,i\}} \partial_y \psi_0 \right), \quad (\text{B13})$$

$$0 = -\partial_y \left(\partial_y M_0^{\{H,i\}} + m_0^{\{H,i\}} \partial_y \psi_0 \right). \quad (\text{B14})$$

The lowest order ion flux is $O(1)$. However, the fluxes pertaining to concentrations of $O(\lambda^0)$ vanish, since the radial derivative introduces a factor of $1/\lambda$

$$-\left(\partial_y m_0^{\{H,i\}} + M_0^{\{H,i\}} \partial_y \psi_0 \right)_{y=0} = 0, \quad (\text{B15})$$

$$-\left(\partial_y M_0^{\{H,i\}} + m_0^{\{H,i\}} \partial_y \psi_0 \right)_{y=0} = 0. \quad (\text{B16})$$

The leading order result for the variables $m_0^{\{H,i\}}(y, \vartheta)$, $M_0^{\{H,i\}}(y, \vartheta)$ in the diffuse layer are then given by

$$m_0^{\{H,i\}}(y, \vartheta) = a^{\{H,i\}}(\vartheta) e^{-\psi_0(y, \vartheta)} - b^{\{H,i\}}(\vartheta) e^{\psi_0(y, \vartheta)}, \quad (\text{B17})$$

$$M_0^{\{H,i\}}(y, \vartheta) = a^{\{H,i\}}(\vartheta) e^{-\psi_0(y, \vartheta)} + b^{\{H,i\}}(\vartheta) e^{\psi_0(y, \vartheta)}, \quad (\text{B18})$$

with yet unknown constants. Matching between the diffuse layer and the outer region as $\lim_{y \rightarrow \infty} \{m_0^{\{H,i\}}, M_0^{\{H,i\}}\} = \lim_{r \rightarrow 1} \{\hat{m}_0^{\{H,i\}}, \hat{M}_0^{\{H,i\}}\}$ yields

$$a^{\{H,i\}}(\vartheta) - b^{\{H,i\}}(\vartheta) = \hat{m}_0^{\{H,i\}}(1, \vartheta), \quad (\text{B19})$$

$$a^{\{H,i\}}(\vartheta) + b^{\{H,i\}}(\vartheta) = \hat{M}_0^{\{H,i\}}(1, \vartheta). \quad (\text{B20})$$

The number of constants $a^{\{H,i\}}$, $b^{\{H,i\}}$ in our solutions is larger than the number of equations. One needs to consider the matching of the $O(\lambda)$ solutions in order to

obtain the full lowest order solution. The result of this further matching process are conservation equations for the radial solute fluxes, which we do not derive here for brevity

$$\left(-\partial_r \hat{M}_0^H(r, \vartheta) - \hat{m}_0^H(r, \vartheta) \partial_r \hat{\psi}_0(r, \vartheta)\right)_{r=1} = \alpha_0(\vartheta), \quad (\text{B21})$$

$$\left(-\partial_r \hat{M}_0^i(r, \vartheta) + \hat{m}_0^H(r, \vartheta) \partial_r \hat{\psi}_0(r, \vartheta)\right)_{r=1} = 0, \quad (\text{B22})$$

$$\left(-\partial_r \hat{m}_0^H(r, \vartheta) - \hat{M}_0^H(r, \vartheta) \partial_r \hat{\psi}_0(r, \vartheta)\right)_{r=1} = \alpha_0(\vartheta), \quad (\text{B23})$$

$$\left(\partial_r \hat{m}_0^H(r, \vartheta) - \hat{M}_0^i(r, \vartheta) \partial_r \hat{\psi}_0(r, \vartheta)\right)_{r=1} = 0. \quad (\text{B24})$$

In the inner region, the Poisson-Boltzmann equation is non-singular. It reads up to $O(\lambda^0)$

$$\partial_y^2 \psi_0(y, \vartheta) = -\frac{m_0}{2} = B(\vartheta) \sinh \psi_0(y, \vartheta), \quad (\text{B25})$$

with

$$B(\vartheta) = \left(\hat{M}_0^H(1, \vartheta) + \hat{M}_0^i(1, \vartheta)\right)/2. \quad (\text{B26})$$

This equation, determining the non-equilibrium concentration near the surface, has the same form as the corresponding equilibrium equation. The result for the potential in the diffuse layer is

$$\begin{aligned} \phi_0(y, \vartheta) = & \psi_0(y, \vartheta) + \hat{\psi}_0(1, \vartheta) = \\ & 2 \ln \left[\frac{1 + \gamma(\vartheta) e^{-\sqrt{B(\vartheta)y}}}{1 - \gamma(\vartheta) e^{-\sqrt{B(\vartheta)y}}} \right] + \hat{\psi}_0(1, \vartheta). \end{aligned} \quad (\text{B27})$$

The value of the potential at the outer periphery of the diffuse layer $\hat{\psi}_0(1, \vartheta)$ is determined through the solution of Eqns. (B5-B8). Given $\hat{\psi}_0(1, \vartheta)$, the overall change in potential over the diffuse layer $\Delta\phi_0(\vartheta)$ is according to Eq. (9)

$$\Delta\phi_0(\vartheta) \equiv \psi_0(0, \vartheta) = V_0 - \Delta\phi_s(\vartheta) - \hat{\psi}_0(1, \vartheta). \quad (\text{B28})$$

The voltage drop over the Stern layer is calculated through Eq. (10), which is in terms of inner variables

$$\Delta\phi_s(\vartheta) = -\frac{\lambda_s}{\lambda} \frac{\partial \psi_0(y, \vartheta)}{\partial y} \Big|_{y=0} = \frac{\lambda_s}{\lambda} \sqrt{B(\vartheta)} \frac{\gamma(\vartheta)}{1 - \gamma(\vartheta)^2}. \quad (\text{B29})$$

Insertion of Eq. (B29) into Eq. (B28) yields a transcendental equation for the function $\gamma(\vartheta)$

$$V_0 = \frac{\lambda_s}{\lambda} \sqrt{B(\vartheta)} \frac{\gamma(\vartheta)}{1 - \gamma(\vartheta)^2} + 2 \ln \left[\frac{1 + \gamma(\vartheta)}{1 - \gamma(\vartheta)} \right] + \hat{\psi}_0(1, \vartheta) \quad (\text{B30})$$

which now allows the full determination of the potential in the diffuse layer. In order to calculate the lowest order swimming speed in $\hat{\mathbf{e}}_z$ -direction from the above results

we expand Eq.(22) for small λ . The lowest order result is

$$U_0 = g\lambda^2 \int_0^\infty \int_0^\pi \frac{m_0(y, \vartheta)}{2} [y^2 \partial_y \phi_0(y, \vartheta) \cos \vartheta - y \partial_\vartheta \phi_0(y, \vartheta) \sin \vartheta] \sin \vartheta \, d\vartheta dy. \quad (\text{B31})$$

On inserting Eqns. (B17,B18,26) including the matched constants and using partial integration we find Eq. (29) for the swimming speed. An explicit calculation of U requires the knowledge of the outer fields at $r = 1$. Therefore, the pertaining differential Eqns. (B5-B8) need to be solved with the boundary conditions Eqns. (B9-B12, B21-B24). Also, the potential of the swimmer, V_0 , depends through the charge conservation Eq. (16) on α and must be determined simultaneously with the concentration fields. The whole task can only be done numerically. To this end, we implement an efficient pseudospectral method⁶⁹ where the discretized system of differential equations is solved with the Newton-Raphson method. In radial direction, we use a Chebychev grid with 30 nodes. The grid in angular direction, for $\vartheta = 0 \dots \pi$, is uniformly spaced with 40 nodes.

Appendix C: Analytical approximation for U

In this appendix we provide the details for the approximate swimming speed, which is given in Sec. III B. Due to radial symmetry and the boundary conditions at infinity no ion fluxes arise in the lowest order where $k_1 \approx 0$, $k_2 \approx 0$. Although being a non-equilibrium steady state, the concentrations of ions follow an equilibrium distribution throughout the whole system. Solutions for the outer field variables, far away from the swimmer, are easily determined from Eqns. (B5-B8) with $\hat{\psi}_{0,0} = 0$ to be $\hat{M}_{0,0}^H = 2\delta$, $\hat{M}_{0,0}^i = 2$, $\hat{m}_{0,0}^H = \hat{m}_{0,0}^i = 0$. The indices denote the λ^0 and k_1^0, k_2^0 order. The inner fields of lowest order obey the differential equations

$$0 = -\left(\partial_y m_{0,0}^{H,i} + M_{0,0}^{H,i} \partial_y \phi_{0,0}\right), \quad (\text{C1})$$

$$0 = -\left(\partial_y M_{0,0}^{H,i} + m_{0,0}^{H,i} \partial_y \phi_{0,0}\right), \quad (\text{C2})$$

and the solutions are given by Eqns. (B17,B18) with $a_{0,0}^H = b_{0,0}^H = \delta$, and $a_{0,0}^i = b_{0,0}^i = 1$. The potential $\phi_{0,0}$ is

$$\phi_{0,0}(y) = 2 \ln \left[\frac{1 + \gamma_0 e^{-\sqrt{B_0 y}}}{1 - \gamma_0 e^{-\sqrt{B_0 y}}} \right], \quad (\text{C3})$$

with $B_0 = \delta + 1$ and $\gamma_0 = \tanh(\phi_{0,0}(0)/4)$.

For the outer variables of first order in k_1, k_2 we demand $\hat{m}_{0,1}^i = -\hat{m}_{0,1}^H$, as in App. B. The field equations read

$$\nabla^2 \hat{M}_{0,1}^H = \nabla^2 \hat{M}_{0,1}^i = 0, \quad (\text{C4})$$

$$\nabla^2 \hat{m}_{0,1}^H = \nabla^2 \hat{\psi}_{0,1} = 0. \quad (\text{C5})$$

The corresponding boundary conditions are

$$\begin{aligned}
-\partial_r \hat{M}_{0,1}^H|_{r=1} &= \alpha_{0,1}, \\
-\partial_r \hat{M}_{0,1}^i|_{r=1} &= 0, \\
-\left(\partial_r \hat{m}_{0,1}^H - 2\delta \partial_r \hat{\psi}_{0,1}\right)|_{r=1} &= \alpha_{0,1}, \\
\left(\partial_r \hat{m}_{0,1}^H - 2\partial_r \hat{\psi}_{0,1}\right)|_{r=1} &= 0 \\
\hat{M}_{0,1}^H|_{r=\infty} = \hat{M}_{0,1}^i|_{r=\infty} = \hat{m}_{0,1}^H|_{r=\infty} &= 0, \\
\hat{\psi}|_{r=\infty} &= 0.
\end{aligned} \tag{C6}$$

Taken together, these equations yield

$$\hat{M}_{0,1}^i = 0, \tag{C7}$$

$$\hat{M}_{0,1}^H = \sum_{n=0}^{\infty} A_n P_n(\cos \vartheta) r^{-n-1}, \tag{C8}$$

$$\hat{m}_{0,1}^H = \hat{M}_{0,1}^H/(\delta + 1), \tag{C9}$$

$$\hat{\psi}_{0,1} = \hat{M}_{0,1}^H/(2\delta + 2), \tag{C10}$$

where the the coefficients of the expansion in Legendre polynomials $P_n(\cos \vartheta)$ are calculated from

$$-\partial_r \hat{M}_{0,1}^H|_{r=1} = \sum_{n=0}^{\infty} (n+1) A_n P_n(\cos \vartheta) = \alpha_{0,1}. \tag{C11}$$

For the corresponding inner variables of first order in k_1, k_2 we have the differential equations

$$0 = -\left(\partial_y m_{0,1}^{H,i} + M_{0,1}^{H,i} \partial_y \phi_{0,0} + M_{0,0}^{H,i} \partial_y \phi_{0,1}\right), \tag{C12}$$

$$0 = -\left(\partial_y M_{0,1}^{H,i} + m_{0,1}^{H,i} \partial_y \phi_{0,0} + m_{0,0}^{H,i} \partial_y \phi_{0,1}\right), \tag{C13}$$

which result in

$$m_{0,1}^{H,i} = a_{0,1}^{H,i} e^{-\phi_{0,0}} - b_{0,1}^{H,i} e^{\phi_{0,0}} - \phi_{0,1} M_{0,0}^{H,i}, \tag{C14}$$

$$M_{0,1}^{H,i} = a_{0,1}^{H,i} e^{-\phi_{0,0}} + b_{0,1}^{H,i} e^{\phi_{0,0}} - \phi_{0,1} m_{0,0}^{H,i}. \tag{C15}$$

Matching now as $\lim_{y \rightarrow \infty} M_{0,1}^{H,i} = \hat{M}_{0,1}^{H,i}|_{r=1}$, $\lim_{y \rightarrow \infty} m_{0,1}^{H,i} = \hat{m}_{0,1}^H|_{r=1}$, $\lim_{y \rightarrow \infty} \phi_{0,1} = \hat{\psi}_{0,1}|_{r=1}$ we find $b_{0,1}^i = -a_{0,1}^i = 0$, $b_{0,1}^H = 0$ and

$$a_{0,1}^H = \sum_{n=0}^{\infty} A_n P_n(\cos \vartheta). \tag{C16}$$

This yields for the H^+ concentration at the outer edge of the compact layer

$$c_{0,1}^{H+} = \frac{M_{0,1}^H + m_{0,1}^H}{2} = (a_{0,1}^H - \delta \phi_{0,1}) e^{-\phi_{0,0}}. \tag{C17}$$

Having obtained the concentration of cations at the surface of the swimmer, we are now in the position to calculate the reaction rate $\alpha_{0,1}$ in first order of k_1, k_2 . We insert $c_0^{H+} \approx \delta e^{-\phi_{0,0}} + c_{0,1}^{H+}$ in Eq. (23) and employ Eq. (30) for the lowest order reaction rate. The boundary

condition for the potential Eq. (31) in order k_1^0, k_2^0 is also employed along with the corresponding also in first order Stern layer boundary condition

$$V_{0,1} = \phi_{0,1}(0, \vartheta) + \Delta \phi_{s,1}(\vartheta) \tag{C18}$$

to yield

$$\alpha_{0,1} = e^{\frac{\Delta \phi_{s,0}}{2}} \left(-\frac{a_{0,1}^H K_2}{\delta} + K_2 V_{0,1} - \cos \vartheta \left(k_2 + k_1 \frac{K_2}{K_1} \right) \right). \tag{C19}$$

This expression along with Eqns. (C11, C16) allows to determine $a_{0,1}^H$. Since the swimmer can not emit a net flux of cations, we demand that the radially symmetric part of $\alpha_{0,1}$ vanishes. Therefore we find with Eqns. (C11, C16), $A_0 = 0$, $V_{0,1} = 0$, and

$$a_{0,1}^H = -\delta \frac{k_2 + k_1 \frac{K_2}{K_1}}{2\delta e^{-\frac{\Delta \phi_{s,0}}{2}} + K_2} \cos \vartheta. \tag{C20}$$

In order to calculate the swimming speed we first consider the body force in the diffuse layer

$$m_0 \nabla \phi_0 \approx m_{0,0} \nabla \phi_{0,0} + (m_{0,1}^H + m_{0,1}^i) \hat{\mathbf{e}}_r \partial_r \phi_{0,0} + (1 + \delta)(e^{-\phi_{0,0}} - e^{\phi_{0,0}}) \nabla \phi_{0,1}. \tag{C21}$$

The first, lowest order term is radially symmetric and therefore irrelevant for the swimming. On inserting the expressions for $m_{0,1}$, we find

$$m_0 \nabla \phi \approx m_{0,0} \nabla \phi_{0,0} + a_{0,1}^H e^{-\phi_{0,0}} \hat{\mathbf{e}}_r \partial_r \phi_{0,0} + (1 + \delta) \nabla ((e^{-\phi_{0,0}} - e^{\phi_{0,0}}) \phi_{0,1}). \tag{C22}$$

Since the last term in the body force is a gradient it only modifies the hydrodynamic pressure and does cause motion of the swimmer in the incompressible limit. Therefore, the first order potential $\phi_{0,1}$ is irrelevant for the swimming speed. Inserting Eq. (C22) with Eq. (C20) into Eq. (B31), we find the formula for the swimming speed up to first order in the asymmetry of surface reactivity given in the main text.

¹P. Mitchell, *Proc. R. Phys. Soc. Edinb.* **25**, 32 (1956)

²P. E. Lammert, J. Prost, and R. Bruinsma, *J. Theor. Biol.* **178**, 387 (1996)

³W. R. Browne and B. L. Feringa, *Nat. Nanotechnol.* **1**, 25 (2006)

⁴S. J. Ebbens and J. R. Howse, *Soft Matter* **6**, 726 (2010)

⁵R. F. Ismagilov, A. Schwartz, N. Bowden, and G. M. Whitesides, *Angew. Chem. Int. Ed.* **41**, 652 (2002)

⁶W. F. Paxton, A. Sen, and T. E. Mallouk, *Chem. Eur. J.* **11** (2005)

⁷S. Fournier-Bidoz, A. C. Arsenault, I. Manners, and G. A. Ozin, *Chem. Commun.*, 441(2005)

⁸J. R. Howse, R. A. L. Jones, A. J. Ryan, T. Gough, R. Vafabakhsh, and R. Golestanian, *Phys. Rev. Lett.* **99**, 48102 (2007)

⁹A. Erbe, M. Zientara, L. Baraban, C. Kreidler, and P. Leiderer, *J. Phys.: Condens. Matter* **20**, 404215 (2008)

¹⁰J. Vicario, R. Eelkema, W. R. Browne, A. Meetsma, R. M. La Crois, and B. L. Feringa, *Chem. Commun.*, 3936(2005)

- ¹¹N. Mano and A. Heller, *J. Am. Chem. Soc.* **127**, 11574 (2005)
- ¹²M. M. Hanczyc, T. Toyota, T. Ikegami, N. Packard, and T. Sugawara, *J. Am. Chem. Soc.* **129**, 9386 (2007)
- ¹³S. Thutupalli, R. Seemann, and S. Herminghaus, *New J. Phys.* **13**, 073021 (2011)
- ¹⁴G. Volpe, I. Buttinoni, D. Vogt, H. J. Kümmerer, and C. Bechinger, *Soft Matter* **7**, 8810 (2011)
- ¹⁵R. Golestanian, T. B. Liverpool, and A. Ajdari, *Phys. Rev. Lett.* **94**, 220801 (2005)
- ¹⁶G. Rückner and R. Kapral, *Phys. Rev. Lett.* **98**, 150603 (2007)
- ¹⁷S. Thakur and R. Kapral, *J. Chem. Phys.* **135**, 024509 (2011)
- ¹⁸B. Sabass and U. Seifert, *Phys. Rev. Lett.* **105**, 218103 (2010)
- ¹⁹B. Sabass and U. Seifert, *J. Chem. Phys.* **136**, 064508 (2012)
- ²⁰G. A. Ozin, I. Manners, S. Fournier-Bidoz, and A. Arsenault, *Adv. Mater.* **17**, 3011 (2005)
- ²¹T. R. Kline, W. F. Paxton, T. Mallouk, and A. Sen, *Angew. Chem.* **117**, 754 (2005)
- ²²S. Balasubramanian, D. Kagan, C. Jack Hu, S. Campuzano, M. J. Lobo-Castañón, N. Lim, D. Y. Kang, M. Zimmerman, L. Zhang, and J. Wang, *Angew. Chem. Int. Ed.* **50**, 4161 (2011)
- ²³L. Baraban, M. Tasinkevych, M. N. Popescu, S. Sanchez, S. Dietrich, and O. G. Schmidt, *Soft Matter* **8**, 48 (2012)
- ²⁴R. Golestanian, *Phys. Rev. Lett.* **102**, 188305 (2009)
- ²⁵J. Palacci, C. Cottin-Bizonne, C. Ybert, and L. Bocquet, *Phys. Rev. Lett.* **105**, 88304 (2010)
- ²⁶B. ten Hagen, S. Van Teeffelen, and H. Löwen, *J. Phys.: Condens. Matter* **23**, 194119 (2011)
- ²⁷Y. Yang, V. Marceau, and G. Gompper, *Phys. Rev. E* **82**, 031904 (2010)
- ²⁸G. V. Kolmakov, V. V. Yashin, S. P. Levitan, and A. C. Balazs, *PNAS* **107**, 12417 (2010)
- ²⁹D. Kagan, S. Balasubramanian, and J. Wang, *Angew. Chem. Int. Ed.* **50**, 503 (2011)
- ³⁰J. Bialké, T. Speck, and H. Löwen, arXiv:1112.5281v1
- ³¹S. Qian and S. W. Joo, *Langmuir* **24**, 4778 (2008)
- ³²J. Elgeti and G. Gompper, *EPL* **85**, 38002 (2009)
- ³³M. N. Popescu, S. Dietrich, and G. Oshanin, *J. Chem. Phys.* **130**, 194702 (2009)
- ³⁴J. L. Anderson, *Annu. Rev. Fluid Mech.* **21**, 61 (1989)
- ³⁵S. Ebbens and J. Howse, *Langmuir* **27**, 12293 (2011)
- ³⁶J. G. Gibbs and Y. P. Zhao, *Appl. Phys. Lett.* **94**, 163104 (2009)
- ³⁷Y. Mei, A. Solovev, S. Sanchez, and O. Schmidt, *Chem. Soc. Rev.* **40**, 2109 (2011)
- ³⁸B. U. Felderhof, *J. Chem. Phys.* **133**, 064903 (2010)
- ³⁹W. F. Paxton, P. T. Baker, T. R. Kline, Y. Wang, T. E. Mallouk, and A. Sen, *J. Am. Chem. Soc.* **128**, 14881 (2006)
- ⁴⁰Y. Wang, R. M. Hernandez, D. J. Bartlett Jr, J. M. Bingham, T. R. Kline, A. Sen, and T. E. Mallouk, *Langmuir* **22**, 10451 (2006)
- ⁴¹W. F. Paxton, K. C. Kistler, C. C. Olmeda, A. Sen, S. K. St. Angelo, Y. Cao, T. E. Mallouk, P. E. Lammert, and V. H. Crespi, *J. Am. Chem. Soc.* **126**, 13424 (2004)
- ⁴²R. Laocharoensuk, J. Burdick, and J. Wang, *ACS nano* **2**, 1069 (2008)
- ⁴³S. Sundararajan, P. E. Lammert, A. W. Zudans, V. H. Crespi, and A. Sen, *Nano Lett.* **8**, 1271 (2008)
- ⁴⁴E. Yariv, *Proc. R. Soc. A* **467**, 1645 (2011)
- ⁴⁵J. L. Moran, P. Wheat, and J. D. Posner, *Phys. Rev. E* **81**, 065302 (2010)
- ⁴⁶J. L. Moran and J. D. Posner, *J. Fluid Mech.* **1**, 1 (2011)
- ⁴⁷D. A. Saville, *Annu. Rev. Fluid Mech.* **9**, 321 (1977)
- ⁴⁸A. V. Delgado, F. Gonzalez-Caballero, R. J. Hunter, L. K. Koopal, and J. Lyklema, *Pure Appl. Chem.* **77**, 1753 (2005)
- ⁴⁹M. Teubner, *J. Chem. Phys.* **76**, 5564 (1982)
- ⁵⁰S. B. Hall, E. A. Khudaish, and A. L. Hart, *Electrochim. Acta* **43**, 579 (1997)
- ⁵¹G. Bianchi, F. Mazza, and T. Mussini, *Electrochim. Acta* **7**, 457 (1962)
- ⁵²J. Newman and K. Thomas-Alyea, *Electrochemical systems* (Wiley-Interscience New York, 2004)
- ⁵³A. Bonnefont, F. Argoul, and M. Z. Bazant, *J. Electroanal. Chem.* **500**, 52 (2001)
- ⁵⁴P. M. Biesheuvel, M. Van Soestbergen, and M. Z. Bazant, *Electrochim. Acta* **54**, 4857 (2009)
- ⁵⁵R. J. Hunter, L. R. White, and D. Y. C. Chan, *Foundations of colloid science*, Vol. 1 (Clarendon press Oxford, 1987)
- ⁵⁶K. T. Chu and M. Z. Bazant, *Phys. Rev. E* **74**, 011501 (2006)
- ⁵⁷S. S. Dukhin, E. Matijevic, and B. V. Derjaguin, *Surface and Colloid Science: Vol. 7* (Wiley-Interscience New York, 1974)
- ⁵⁸D. C. Prieve, J. L. Anderson, J. P. Ebel, and M. E. Lowell, *J. Fluid Mech.* **148**, 247 (1984)
- ⁵⁹H. Wang and L. Pilon, *J. Phys. Chem. C* **115**, 16711 (2011)
- ⁶⁰<http://www.h2o2.com/technical-library/physical-chemical-properties>, website of U.S. Peroxide, LLC
- ⁶¹F. Carrique and E. Ruiz-Reina, *J. Phys. Chem. B* **113**, 8613 (2009)
- ⁶²C. S. Mangelsdorf and L. R. White, *J. Chem. Soc., Faraday Trans.* **86**, 2859 (1990)
- ⁶³D. C. Grahame, *J. Am. Chem. Soc.* **76**, 4819 (1954)
- ⁶⁴J. J. Bikerman, *Trans. Faraday Soc.* **35**, 154 (1940)
- ⁶⁵A. Ajdari and L. Bocquet, *Phys. Rev. Lett.* **96**, 186102 (2006)
- ⁶⁶A. V. Belyaev and O. I. Vinogradova, *Phys. Rev. Lett.* **107**, 098301 (2011)
- ⁶⁷Y. Mukoyama, H. Hommura, S. Nakanishi, T. Nishimura, H. Konishi, and Y. Nakato, *Bull. Chem. Soc. Jpn.* **72**, 1247 (1999)
- ⁶⁸S. B. Hall, E. A. Khudaish, and A. L. Hart, *Electrochim. Acta* **43**, 2015 (1998)
- ⁶⁹J. P. Boyd, *Chebyshev and fourier spectral methods* (Springer-Verlag Berlin, Heidelberg, 1989)